Journal of Marine Research, 52, 1017–1036, 1994

Currents under land-fast ice in the Canadian Arctic Archipelago Part 1: Vertical velocities

by R. F. Marsden[1], R. Paquet[1] and R. G. Ingram[2]

ABSTRACT

A 614 kHz acoustic Doppler current profiler was deployed through land-fast ice in Resolute Passage, in the Canadian Archipelago for 30 days in April and May 1992. It was demonstrated that in the mean, at tidal and at high frequencies the instrument was stable and aligned within 0.5° of vertical, permitting unambiguous measurement of the horizontal, and more importantly, the vertical velocity structure. The flow was dominated by tidal and high frequency (15 min period) oscillations. The K_1 and M_2 tidal currents were both approximately 10.0 cm s^{-1}, oriented along-channel. The K_1 component was constant with depth while the M_2 component changed in magnitude and its sense of rotation. The corresponding vertical velocities showed maximum spectral power density in the semi-diurnal frequency band but were insignificant in the diurnal band. At high frequencies, 31 events, or groups of oscillations with vertical velocities greater than 3.5 cm s^{-1} were found. They were identified as finite amplitude internal waves trapped to the pycnocline, finite amplitude internal waves at greater depth (corresponding to a change in the density structure) and linear internal waves. The horizontal kinetic energy of the oscillations was dependent on the spring-neap tidal cycle. It is proposed that many were generated through interaction of the tidal flow with a compression ridge in the ice, located approximately 15 km from the measurement site.

1. Introduction

The acoustic Doppler current profiler (ADCP) has taken an increasingly important role in the investigation of ocean currents. Unwanted movement of the transducer head due to ship motion for vessel mounted (VM) configurations and mooring motion for bottom mounted systems can, however, seriously contaminate readings. For example, Greenwood *et al.* (1993), in an intercomparison with cyclesondes calculate an actual rms error of 3.9 cm s^{-1} for a VM 150 kHz ADCP compared to a nominal rms error of 0.8 cm s^{-1} suggested by the manufacturer. The implication is that ship motion can reduce the signal-to-noise ratio by a factor of about 25. Consequently, horizontal velocities only are cited for VM systems. Should the instrument platform be stabilized, however, direct measurement of the vertical velocity may be possible.

1. Physics Department, Royal Roads Military College, FMO, Victoria, B.C., Canada, V0S 1B0.
2. Department of Atmospheric and Oceanic Sciences, McGill University, 805 Sherbrooke Street West, Montreal, Quebec, Canada, H3A 2K6.

The vertical velocity (w) is the absolute signature of internal waves and is of paramount importance. Previous studies, (e.g. Petrie, 1975; Drakopoulos and Marsden, 1993), have only inferred w through the temporal evolution of temperature or salinity surfaces. In coastal regions, however, inferred vertical velocities from passive scalars can be contaminated through the advection of large horizontal gradients and mixing. During April–May 1992, we participated in a joint Canadian-Japanese project (the SARES project), attempting to identify factors that influence the "biological pumping" of CO_2 under first-year ice-covered seas, i.e. the production and export of microscopic algae that grow within the ice-matrix and at the ice-water interface (Horner *et al.*, 1992). The study offered an opportunity to deploy an ADCP suspended through land-fast ice near Resolute Bay, NWT. It was hoped that this stable platform would permit unequivocal measurement of vertical velocity profiles.

One month of data were obtained and the complete velocity field, including the vertical component, was sampled in 2 m depth bins, from 3 to 51 m below the ice, every 2 min. It will be shown that w was an extremely sensitive indicator of numerous instances of high frequency (periods <1 hour) vertical velocity events lasting from 1 to 10 hours. The measurements indicated two distinct high frequency regimes: moderately non-linear internal waves which we will show are consistent with the theory of internal solitons and linear high frequency internal waves. Our results are unique because we have detected, to our knowledge, the first unambiguous measurement in field conditions of the vertical velocity structure of linear internal waves and finite amplitude internal waves. Furthermore, the spatial and temporal resolution achieved for the three velocity components has never been presented in the literature. The purpose of this paper is to present a thorough description of the details of the measurements and to indicate the range of internal oscillations found. The vertical velocity is extremely difficult to detect with certainty and the veracity of our results will depend critically on demonstrating that proper alignment of the ADCP was maintained, ensuring that our measurements do not reflect a rotation of the large horizontal velocity component into the vertical. Consequently, we will show that, in the mean, at tidal frequencies, and at high frequencies, our results are consistent with the correct alignment and stability of the instrument. The paper will be organized in the following manner. Section 2 will contain a discussion of the experimental design. Since the flow is tidally dominated, Section 3 will examine the raw record and focus on the mean and tidal oscillations. Section 4 will present an overview of the range of high frequency oscillations that were found in the record. Section 5 will present a discussion of the results and concluding remarks.

2. Experimental design

Arguments confirming the reliability of our w estimates require a rudimentary knowledge of the ADCP. Our instrument consists of four transducers mounted at 30°

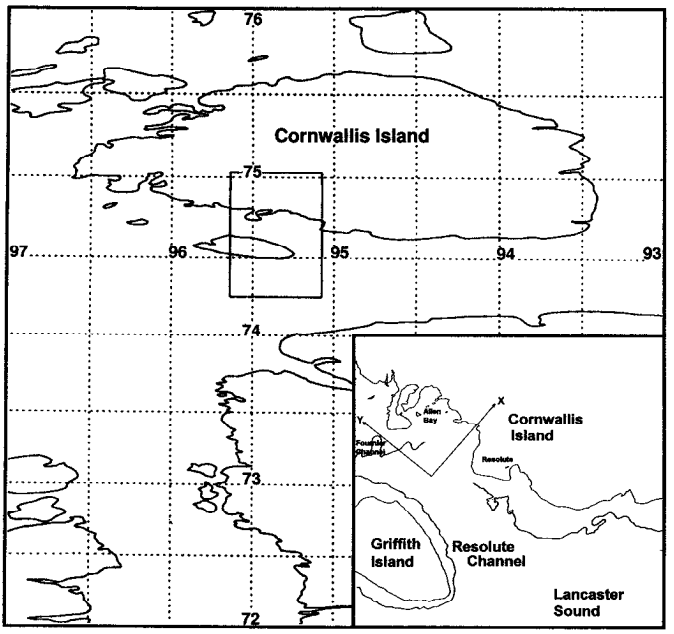

Figure 1. The study location, local topography (inset) and axes definitions used in the paper.

to the horizontal. An outgoing pulse (or "ping") is emitted from each of the beams which is then reflected off the center of mass of zooplankton and other reflectors in the water column. The Doppler shift of the return echo is range gated to determine the relative velocity difference between the water parcel and the instrument as a function of depth. Simple trigonometric identities convert the radial velocities to orthogonal Cartesian coordinates (u, v and w). Two independent estimates of the vertical velocity (w) are calculated for each ping. The recorded w is the mean of the two values while an error velocity (e) is also defined which is the difference in the two. An individual acoustic emission has a large intrinsic error. Consequently, a large number of pings are averaged for typically a minute or more to increase the statistical reliability of the estimate. If a w estimate is much larger than the standard deviation of e (σ_e) then it is statistically significant.

The study took place from 21 April to 25 May 1992 at 74°41.19'N 95° 15.59'W, approximately 10 km south-west of the village of Resolute Bay on land-fast ice in Resolute Passage (Fig 1). The water was 135 m deep and the ice was 1.8 m thick, through which a 1.2 m by 1.8 m hole was cut to allow for the deployment of equipment including the ADCP and a Conductivity, Temperature and Depth (CTD) probe. An insulated tent, kept at approximately 20° C, was erected over the hole for the duration of the study. The transducer from our RDI VM 614 kHz ADCP was attached to a 2.5 m steel pole, 10 cm in diameter suspended from a steel frame through the deployment hole, perpendicular to the bottom of the ice (see Fig. 2). The

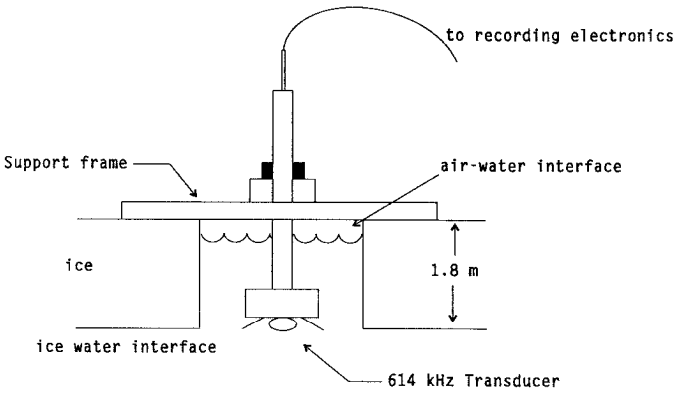

Figure 2. Diagram of the instrument installation.

pole was gimballed in one direction and was set to plumb using a carpenter's level and verified through comparison with a plumb line. The weight of the head (50 kg) and steel pole ensured that the system remained vertical. The concave VM transducer head was designed to fit into a sea chest and provided two major advantages for our study. First, it could be recessed into the hole so that the transducers were aligned with the ice-water interface and no part of the equipment protruded into the flow field. Second, it allowed for 0.5 m of ice growth (in fact, only 5 cm was observed) before the hole interfered with the acoustic beams. It was immediately apparent that the head did not interact with the flow. Every morning the assembly was re-calibrated for plumb and the frazil ice was examined for any disruption due to pole drift. None was found and no readjustment of the system was required after the initial set-up. Further evidence of the stability and alignment of the system will be presented in the post-deployment calculations.

CTD profiles were measured at approximately noon each day using a Sea-Bird SBE-19 profiler. An evaluation of the initial cast indicated that the minimum buoyancy period was approximately 4.5 min. Since this is the minimum allowable internal wave period, the ADCP sampling was set to 2 min to ensure adequate temporal sampling. The spatial sampling was set to 25 depth bins of 2 m each from 3 to 51 m depth below the ice edge. The three velocity components, the return signal strength and the percentage of fully detected acoustic reflections for each depth bin were logged on a micro-computer. The number of emissions for each ensemble was constant at 98 while the percent of good returns was typically greater than 98% to 51 m depth. Under these conditions, the nominal RMS error of the 614 kHz transducer, was 0.72 cm s^{-1} for the vertical velocity and 1.26 cm s^{-1} for the horizontal components. As indicated in Figure 1, the positive y direction is along channel at 310° clockwise from true north, the positive x axis is oriented at 40° true and the z axis is positive downward from the water-ice interface. All times are Central Standard Time and will be cited in fractions of an hour to conform to computer drawn figures.

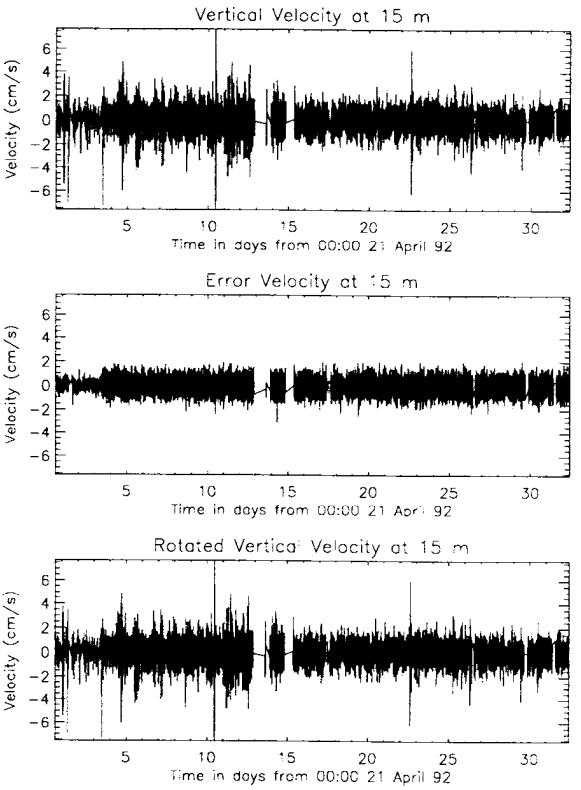

Figure 3. Vertical velocity w (a), error velocity (b) and the vertical velocity of (a) rotated 4° in the $u - w$ plane about the v axis measured at 15 m below the ice-water interface (c). Note the corruption of w in (c) by the horizontal component.

3. Low frequency flow

a. Mean flow. Figures 3a and b show the vertical and error velocities respectively, sampled at 15 m depth. Both time series exhibit a black mat between ± 1.5 cm s^{-1}, roughly twice that of the expected instrument error. From the start of the record to 23 Apr 92, we used a 5 min sampling period, reflected in the reduced noise indicated initially in the error velocity. The vertical velocity channel shows a number of "spikes" rising well above the noise level that are not present in the error velocity, indicating that they should be regarded as signal. Figure 3c shows the vertical velocity after rotation of 4.0° in the $u - w$ plane about the v axis. The rotated vertical velocities exhibit distinct interference from the horizontal tidal velocities. We include this figure to emphasize the signature of a corrupted signal for a very small rotation angle. At no time during the record did our unrotated velocities (Fig. 3a) display mapping of the horizontal tidal flow into the vertical component.

Figure 4 contains a sample of the raw time series for the along-channel (Fig. 4a) and cross-channel (Fig. 4b) velocities sampled at 15 m depth. The along-channel flow

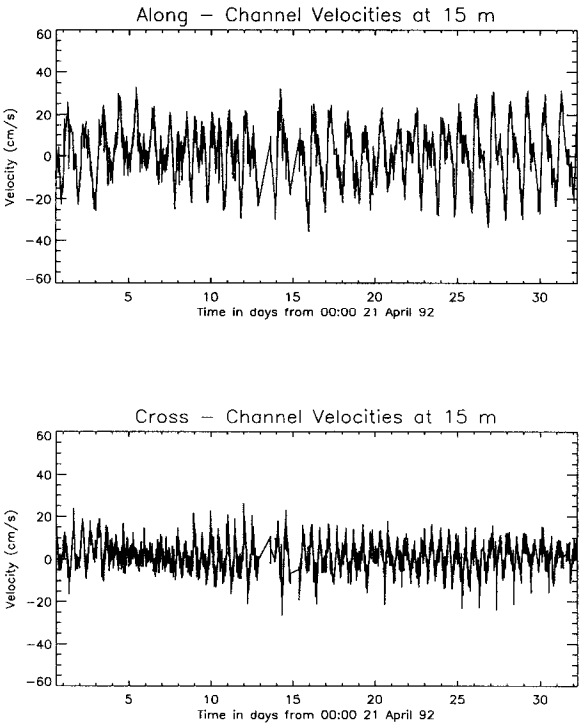

Figure 4. Example of the along-channel, v (a) and cross-channel, u (b) velocities measured at 15 m below the ice-water interface.

is tidally dominated and shows considerably more variability than the cross-channel component. The mean and standard deviations of the flow for the along-channel, cross-channel, vertical and error velocities, calculated from all the available data at each depth, appear in Figures 5a and b respectively. The error bars cited are ± 2 standard errors of the mean accounting for the autocorrelation of the data following Bayley and Hammersley (1946). The horizontal mean flow ($<u>$ and $<v>$) is small, < 4.0 cm s^{-1}, directed southeast along the channel. The along-channel velocity variance increases with depth and is an order of magnitude larger than that of the cross-channel component, consistent with the raw time series of Figure 4.

The mean vertical velocity ($<w>$) is significant with maximum upward values of 0.1 cm s^{-1} near the surface and at 51 m depth. The large mean values are not due to instrument mis-alignment. It was determined that a rotation of 4.0° about the z axis produced the lowest mean vertical velocity. The effects of such a rotation were shown in Figure 3c and were clearly inappropriate. Marsden *et al.* (1994a, Part 2 to this paper) will show that during the passage of these high frequency 'spikes,' simultaneous CTD casts indicated a net transport of water properties from the pycnocline to

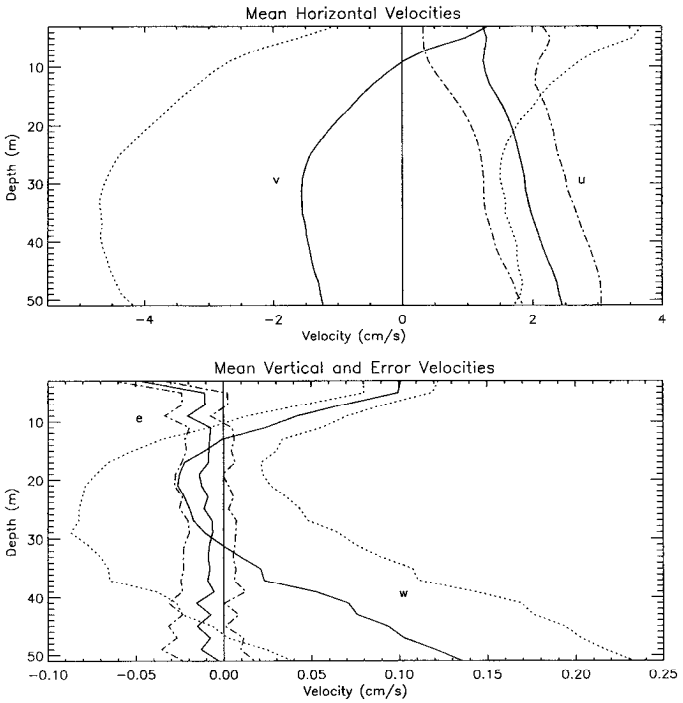

Figure 5. Mean (solid lines) ±2 standard deviations for the horizontal velocities (a); vertical and error velocities (b).

the ice-water interface, due to internal wave breaking, that is consistent with the upward mean flow shown in the figure. If the vertical velocity associated with the eddies were symmetric, there would be no trapping at the ice-water interface. Furthermore, an analysis of the Richardson number indicates that the regions immediately above and below the pycnocline are susceptible to internal instabilities. The first zero crossing in $<w>$ coincides with the pycnocline, exactly where one would expect wave breaking to be suppressed. Figure 3a shows that w has large asymmetric sporadic surges of up to 8.5 cm s^{-1}. There is a clear bias in the 'spikes' to negative velocities in Figure 3a consistent with the negative average at that depth in Figure 5b. Thus, the non-zero means reflect the structure of a few random, large events rather than a long-term mean offset. The mean error velocity ($<e>$) shown in Figure 5b is again very small (~ 0.01 cm s^{-1}), is nearly constant with depth, and in most cases is statistically insignificant. The large mean error velocity at 3 m depth may be due to interference in the electronics between the time taken to change from transmitting the outgoing pulse to receiving, range gating and measuring the Doppler shift of the incoming pulse (see Greenwood, 1991 for a more complete discussion).

More conclusive proof of the stability and alignment of the platform can be found in the eigenstructure of the cross covariance matrix given by

$$\begin{pmatrix} \sigma_u^2 & C_{uv} & C_{uw} \\ C_{uv} & \sigma_v^2 & C_{vw} \\ C_{uw} & C_{vw} & \sigma_w^2 \end{pmatrix} \begin{pmatrix} e_1^i \\ e_2^i \\ e_3^i \end{pmatrix} = \lambda^i \begin{pmatrix} e_1^i \\ e_2^i \\ e_3^i \end{pmatrix} \tag{1}$$

where C_{uv}, for example, is the cross covariance function given by

$$C_{uv} = \frac{1}{N} \sum_{j=0}^{j=N} (u_j - <u>)(v_j - <v>) \tag{2}$$

$\vec{e^i}$ and λ^i are the i^{th} eigenvector and eigenvalue respectively where $\lambda^1 > \lambda^2 > \lambda^3$. The eigenvector corresponding to the smallest eigenvalue (λ^3) will be directed along the axis of minimum velocity variance. The direction of rotation from vertical required to minimize the variance of w is

$$\phi = \tan^{-1}\left(\frac{\sqrt{(e_1^3)^2 + (e_2^3)^2}}{e_3^3}\right). \tag{3}$$

The mean rotation angle was found to be 0.3° with all values $<0.5°$ indicating that the pole was aligned closely with the direction of minimum velocity fluctuation which we take to be vertical.

b. Tidal flow. An harmonic analysis was performed on the data according to Foreman (1979). The inertial frequency (f) is separated from the M_2 by only $1.368 \times 10^{-4}\text{h}^{-1}$ and distinguishing between the two with one month of data is impossible. Consequently, this constituent will be referred to as M_2-f. The largest tidal constituents were the M_2-f and the K_1 and their respective tidal current ellipses at selected depths are shown in Figure 6. The K_1 component is constant with depth, with the exception of a possible Ekman layer near the ice-water interface, suggesting that it is barotropic. The M_2-f component, however, shows considerable variation with depth, changing its sense of rotation through 23 m, indicative of a high degree of baroclinicity. Due to a large number of gaps in the record, Paquet (1993) applied the Lomb-Scargle (Lomb, 1976; Scargle, 1982) Fourier transform to the vertical velocities and found that the semi-diurnal band had the largest power, consistent with its baroclinic nature found in the harmonic analysis. The diurnal band was in the noise level, as one would expect for a barotropic tide. If the instrument head were mis-aligned or oscillating in the flow, the w velocity would have significant power in both the semi-diurnal and diurnal bands since the power in the horizontal velocities in these frequency bands was nearly identical.

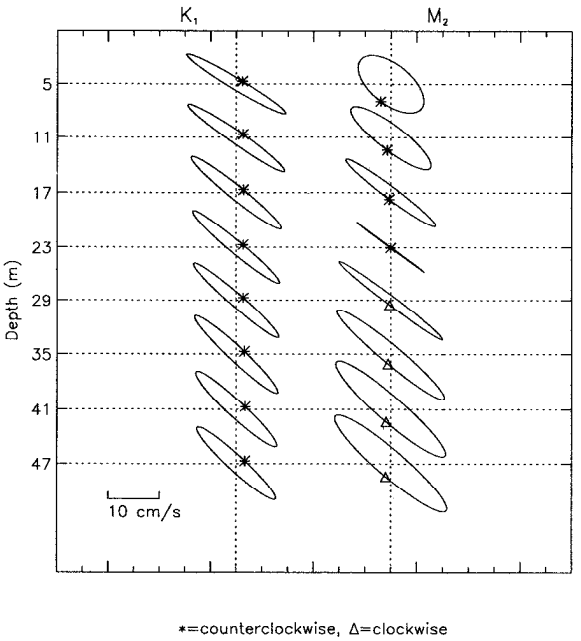

Figure 6. K_1 and M_2-f tidal ellipses at selected depths. The asterisk indicates counterclockwise and the triangle clockwise rotation while its angle, counterclockwise from the x axis indicates the Greenwich phase angle. The direction of the major axis is along-channel.

4. High frequency flow

The horizontal velocities were convolved with a high pass filter having a half power point at one hour and zero power at two hours. The filtered 15 m cross-channel velocity of Figure 4 appears in Figure 7. Similar to the vertical velocities, there is a black mat between ± 2.28 cm s^{-1}, approximately twice the instrument RMS error. Furthermore, there are numerous instances where the velocity rises well above the noise level to as much as ± 28.0 cm s^{-1} corresponding to the 'spikes' in the vertical velocity component of Figure 3a. The horizontal kinetic energy density of the high pass filtered velocity was calculated as

$$KE = \int_{51}^{3} \rho(z) \frac{u_{hp}^2(z) + v_{hp}^2(z)}{2} dz \tag{4}$$

where the subscript *hp* denotes high pass filtered component and u and v are the cross- and along-channel velocity components respectively. The horizontal kinetic energy density of the high pass filtered record appears in Figure 8 and it shows a 14 day spring-neap modulation matching that indicated in the along-channel velocity of Figure 5a. When viewed on an expanded time axis, the 'spikes' could be separated into finite amplitude internal waves and linear internal waves.

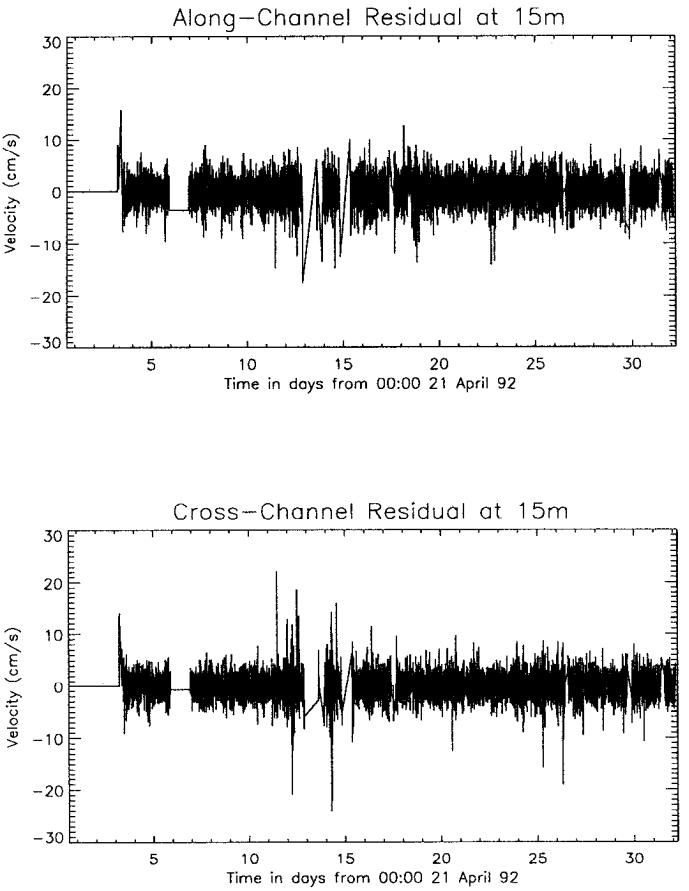

Figure 7. High pass filtered time series of horizontal velocities sampled at 15 m depth (a) along-channel and (b) cross-channel respectively.

a. Response 1—Finite amplitude waves. Figures 9a and b show the vertical and horizontal high pass filtered velocities respectively on an expanded time axis for a 'spike' occurring in the afternoon of 3 May 1992. There is clearly considerable structure in the isotachs. The vertical velocity shows three distinct wavelets each having downward followed by upward motion with zero crossings at 13.8, 14.2 and 14.7 hours (i.e. 24 and 30 min apart) extending from the ice-water interface to below 51 m with the maxima centered at 20 m depth. Maximum downward and upward w are 4.1 and 5.6 cm s^{-1} respectively—well above the 1.4 cm s^{-1} noise level indicated in both the vertical and error velocity time series of Figure 3. The horizontal high pass filtered velocities were rotated in increments of 5° and the variance of the rotated u component calculated. The propagation direction, to within a 180° ambiguity was taken to be the direction of maximum horizontal velocity variance. The absolute direction from the generation region was taken to be opposite to the dominant

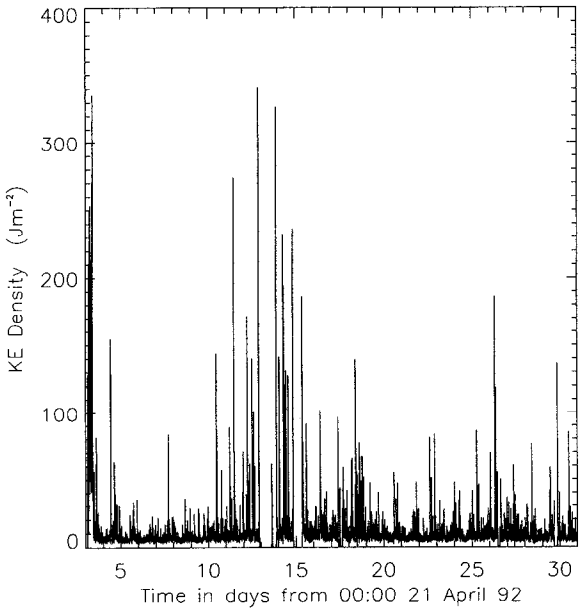

Figure 8. Horizontal kinetic energy density of the horizontal velocities calculated from 51 m depth to the surface.

direction of the velocity contour plot which, for example, in Figure 9b was 255° from north. The isotachs are highly surface trapped with negligible velocities below 20 m depth and maxima at 10 m. If the horizontal velocity components were being mapped into the vertical, one would expect a highly correlated response in both channels. Instead, the horizontal velocities have their maxima at 13.8, 14.2 and 14.7 hours, coincident with the *zero* crossings of the vertical velocity. Furthermore, the horizontal velocities are highly surface trapped with negligible values below 20 m depth, exactly where the vertical velocities have maxima.

The entire record was examined and occurrences of vertical velocities with amplitudes greater than 3.5 cm s^{-1} were noted. They were detected in groups of 3 to 4 wavelets, which we will denote as an event, lasting up to 3 hours. In all, 27 events were observed and their characteristics are listed in Table 1. Prior to 4 May 1992, the vertical velocity maxima were concentrated in the pycnocline at 15–20 m depth. Subsequent events had vertical velocity maxima at 40–50 m depth and horizontal high pass filtered velocities extending to 40 m depth as shown in Figure 10 for event 20 on 5 May 92. This vertical downward migration reflects a change in density structure. Figure 11 shows typical density profiles sampled on 2 and 16 May. Prior to 4 May, there is an unstable region to 10 m depth, a sharp pycnocline between 10 and 20 m with weak stratification at depth. After 4 May, however, there remains an unstable surface layer, but the previously strong pycnocline is non-existent.

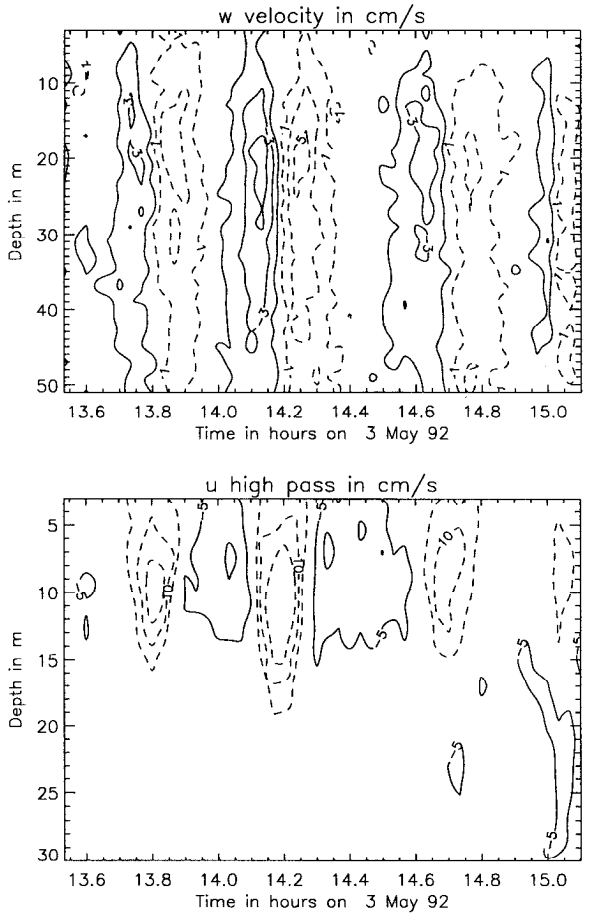

Figure 9. Vertical (a) and rotated horizontal (b) high pass filtered velocities (see text) sampled on 3 May 1992. For (a), the contour interval is 2.0 cm s^{-1} with solid lines corresponding to downward motion and dashed lines corresponding to upward motion. For (b), the contour interval is 5.0 cm s^{-1} with the dash line indicating motion in the positive rotated direction.

Solitons, cnoidal waves, and bores are examples of finite amplitude waves where the steepening effects of amplitude dispersion balance the widening effects of phase dispersion. Solitons have typically been identified through the deflection of isopycnal surfaces (eg. Sandstrom and Elliott, 1984; Cummins and LeBlond, 1984). To this end, we performed an approximate Lagrangian integration of the vertical velocities

$$z_i = z_{i-1} + w_i(z_{i-1})\Delta t \tag{5}$$

where z_i is the location of a particle starting at $z = z_0$, $t = 0$, t is the time step (2 min) and $w_i(z_{i-1})$ is the vertical velocity at time i at the depth of the previous time step z_{i-1}.

Table 1. Synopsis of the 31 high frequency internal waves described in the paper. The arrival direction is the direction from the assumed generator region measured clockwise from geographic north. FA refers to finite amplitude waves.

Event	Starting Time	Duration	# of wavelets	Type of event	Arrival direction
1	00:0022April	4:00hrs	3	FA	320°
2	08:0022April	1:30hrs	1	FA	265°
3	11:1524April	1:45hrs	2	FA	345°
4	11:3025April	10:00hrs	?	Internal Wave	—
5	12:0026April	2:00hrs	4	FA	340°
6	15:3026April	1:30hrs	?	Internal Wave	—
7	13:0027April	7:00hrs	?	Internal Wave	—
8	02:3028April	0:45hrs	1	FA	060°
9	05:5028April	2:20hrs	4	FA	255°
10	16:5028April	0:30hrs	1	FA	300°
11	16:0029April	0:50hrs	2	FA	325°
12	10:0030April	2:00hrs	4	FA	285°
13	10:3001 May	2:30hrs	4	FA	290°
14	17:4001 May	1:00hrs	2	FA	320°
15	18:0002 May	1:24hrs	2	FA	265°
16	04:0003 May	5:00hrs	?	Internal Wave	—
17	13:3803 May	1:24hrs	3	FA	255°
18	00:1505 May	1:30hrs	2	FA	150°
19	06:3005 May	2:30hrs	4	FA	025°
20	10:1505 May	1:10hrs	2	FA	320°
21	08:3006 May	1:30hrs	2	FA	035°
22	09:0007 May	1:00hrs	1	FA	090°
23	18:1509 May	1:45hrs	3	FA	295°
24	14:1513 May	1:30hrs	3	FA	335°
25	21:0013 May	1:30hrs	3	FA	280°
26	05:4516 May	1:15hrs	1	FA	025°
27	00:3017 May	1:15hrs	3	FA	175°
28	07:0017 May	1:45hrs	3	FA	030°
29	08:4019 May	1:10hrs	1	FA	050°
30	10:3020 May	0:45hrs	1	FA	010°
31	15:0021 May	1:00hrs	1	FA	290

This would be equivalent to the displacement of an isopycnal surface if there were no mixing. The Benjamin (1966) model of a Korteweig-de Vries internal solitary wave

$$\eta = A\phi(z)\,\mathrm{sech}^2\left(\frac{x}{\lambda}\right) \tag{6}$$

was fit to the calculated isopycnal surface. Here $\phi(z)$ is the eigenfunction of the Sturm-Liouville problem

$$\frac{\partial}{\partial z}\left(c_\partial^2 \rho \frac{\partial \phi}{\partial z}\right) - g\frac{\partial \rho}{\partial z} = 0 \tag{7}$$

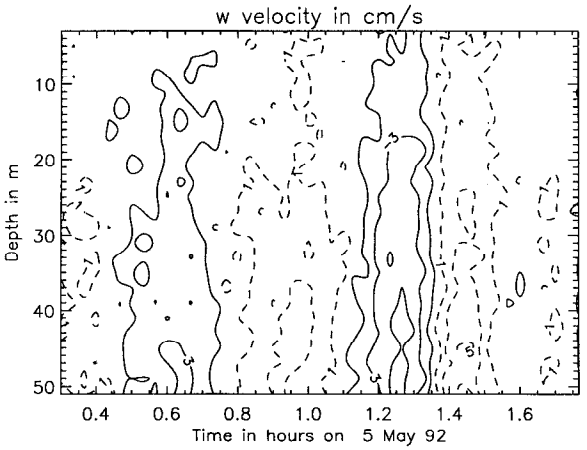

Figure 10. Same as the vertical velocities in Figure 9a for 5 May 1992. Note the downward migration of the isotachs that occurred in the 2 day interval.

where g is the acceleration of gravity and ρ is the mean unperturbed density field and c_0 is the phase speed of an infinitesimally small amplitude shallow water wave. The phase speed (c) and the wavelength (λ) are given by

$$c^2 = c_0^2\left(1 + \frac{A\int_h^0 \rho\phi'^3\,dz}{\int_h^0 \rho\phi'^2\,dz}\right) \tag{8}$$

$$\lambda^2 A = 4\left(\frac{c^2\int_h^0 \rho\phi^2\,dz}{c_0^2\int_h^0 \rho\phi'^3\,dz}\right) \tag{9}$$

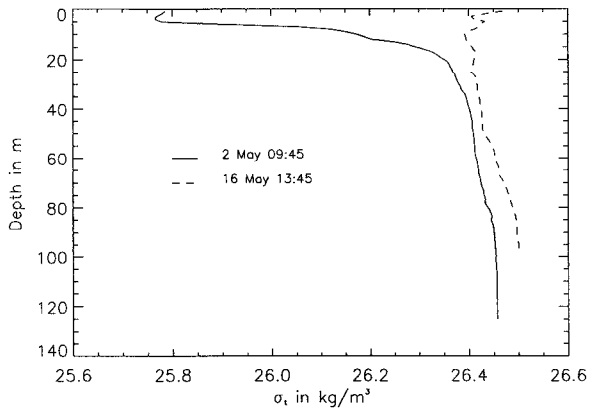

Figure 11. σ_t sampled on 2 May and 16 May, demonstrating typical density profiles before and after 4 May.

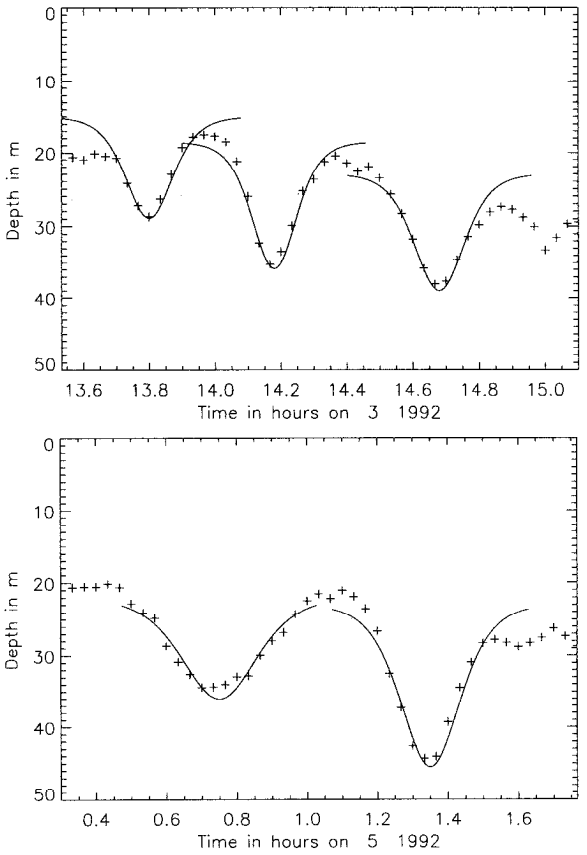

Figure 12. The integrated isopycnal surface depths (crosses) for a water parcel initally at 21 m compared to that predicted by the Benjamin (1966) model for 3 May (a) and 5 May (b).

where c is the phase speed of the solitary wave, and A is its amplitude. Figures 12a and b contain the integrations of the vertical velocities on 3 and 5 May for the parcel initially at 21 m depth corresponding to the vertical velocities of Figures 9 and 10, respectively. Note that the integrated surfaces are cusped downward and do not show an "overshoot," characteristic of linear internal waves. The amplitude of each wavelet was estimated from the data and the Benjamin model was used to determine their spreads and phase speeds based on coincident density structures. The fit is shown as the solid curve in the figure while c and λ appear in Table 2. Although more direct confirmation through direct estimates of the phase speed by separated current meters would supply more conclusive corroboration of solitary wave theory, both the downward cusped shape of the data and the excellent model agreement supports our contention that we have observed some form of finite amplitude internal wave. Various other models were compared to the data including the deep water model of Benjamin (1967) and two-layered versions of both the Benjamin (1966) and Benja-

Table 2. The estimated amplitude and calculated phase speeds and wavelengths used to compare the Benjamin (1966) model to the data shown in Figure 14.

Wavelet	A m	c cm s^{-1}	λ m
3 May			
1	20	30	104
2	23	31	100
3	19	30	105
5 May			
1	19	28	140
2	30	30	120

min (1967) models. All produced waveforms much narrower than indicated by the data. In comparing data to models based on inner and outer expansions of the density field (e.g. Benjamin, 1967; Kubota *et al.,* 1978), the eigenstructures and hence the wave forms were very sensitive to the selected inner regions. The shape parameters could be forced to vary by a factor of 2 by judicious selection of the boundary of density variation. Finally, another commonly cited model, Benny (1966), is identical to Benjamin (1966) to lowest order in the expansion parameter.

The horizontal high pass filtered velocity of four of the events showed a systematic variation with depth. Figure 13 shows the horizontal velocity amplitude and direc-

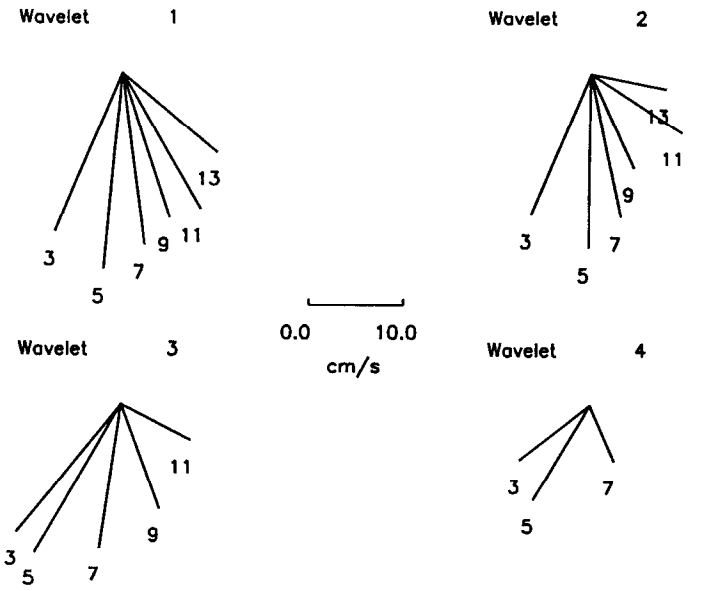

Figure 13. Stick vectors showing the direction of the horizontal high pass filtered velocity components sampled at the time of zero crossing in the vertical velocity for event 13 on 1 May.

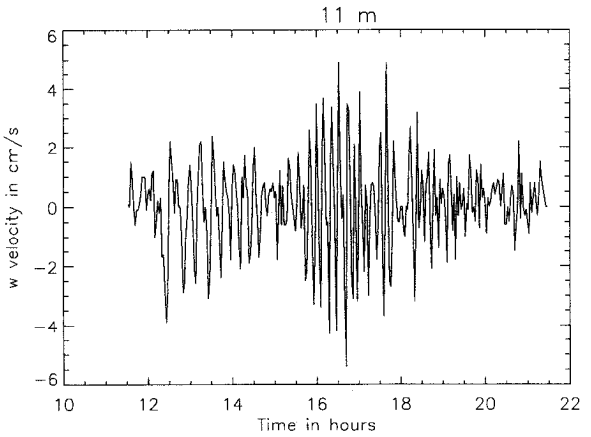

Figure 14. Time series of the vertical velocity at 11 m depth for event 4 on 5 Apr.

tion, coincident with the zero crossing in the vertical velocity, as a function of depth for event 13 sampled on 1 May. Clearly, all four wavelets rotate counter-clockwise with depth through a maximum of 150°. Event 28 (not shown), however, displayed a clockwise rotation through 50° while event 17 (not shown) rotated counter-clockwise through 50°. Heathershaw *et al.* (1987) found a similar rotation in the velocity structure of high frequency internal tide surges that they measured in the Celtic Sea but were unable to explain these features. The existence of both clockwise and counter-clockwise rotations suggests that these may be due to conditions specific to the area such as tidal shear or the three dimensional structure of the generation region rather than due to a systematic dynamic effect such as Ekman rotation.

b. Response 2—Linear internal waves. Table 1 classifies four events as linear internal waves. They are generally of longer duration than the finite amplitude waves. The time series of w measured at 11 m associated with event 4 of 25 April is presented in Figure 14, The total duration of the event is about 10 hours, considerably longer than the 1–3 hours associated with the finite amplitude waves. Rather than 2–4 peaks, it has a minimum of 30 oscillations, highly trapped to the pycnocline, showing a 4 hour modulation. An integration of the vertical velocity (not shown) indicated an "overshoot" and "undershoot" about the equilibrium depth, typical of linear internal waves. Furthermore, Marsden *et al.* (1994b) show that a linear internal wave model can be fit to these data to produce reasonable estimates of internal wave directional spectra. Consequently, we identify this record as a linear internal wave train. Comparison of Table 1 with Figure 4 indicates that they occur during neap tides.

The power spectral densities of the vertical velocities and the high pass filtered horizontal velocities were calculated by dividing the record into 9 groups of 33 points which were fast Fourier transformed and averaged. The results for the vertical velocities appear in Figure 15. The spectral peak is clearly evident at 0.0015 Hz with

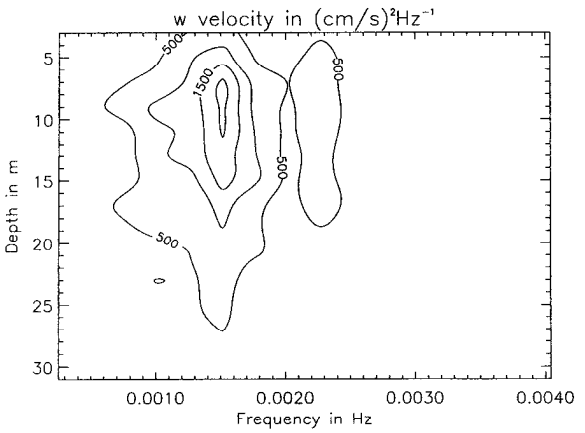

Figure 15. Contour of the power spectral density of the vertical velocity as function of depth for event 4 on 5 Apr.

a maximum in the pycnocline at 8 to 12 m. There is a suggestion of a secondary maximum at 0.0022 Hz. The maximum of the cross-channel velocity power spectral density (not shown) is also at 0.0015 Hz and is highly surface trapped (above 5 m depth). The along-channel velocity spectral power density (not shown and also highly surface trapped) is much lower than that of the cross-channel component, suggesting that the dominant internal wave propagation is cross-channel. The distinct difference between the distribution of spectral power density of the vertical and horizontal velocities again indicates that the two are separate with no suggestion of instability or mis-alignment of the instrument.

5. Discussion and conclusions

We have presented initial results from the deployment of an ADCP through land-fast ice in the Canadian Arctic. Based on the work of Greenwood *et al.* (1993), our objective was to obtain reliable estimates of the vertical velocity. Particular attention was paid to ensure that the instrument was both vertical and stable. A post-analysis of the data indicated that these conditions were achieved. First, an eigenvector analysis showed that the direction of minimum variability was less than 0.5° from vertical. Next, the horizontal component of the flow was found to be tidally dominated with the K_1 and the M_2-f constituents being of equal amplitude. The K_1 constituent was barotropic while the M_2-f showed considerable variation with depth. The Fourier transform of the vertical velocity indicated that there was considerable power in the semi-diurnal band while that of the diurnal band was in the noise. If the horizontal components were being mapped into the vertical, both frequency bands would have significant spectral power density. Finally, the record indicated numerous high frequency oscillations. The maxima in the horizontal velocities co-occurred

with zero crossings in the vertical velocities. Furthermore, the horizontal velocity was surface trapped, while the vertical velocity was a maximum in the pycnocline further demonstrating the independence between the measurements of the vertical and horizontal components of the velocity field.

The record of the high frequency component of the flow indicated two basic structures, finite amplitude internal waves and linear internal waves. Their production was clearly tidally driven as the horizontal kinetic energy density of the high pass filtered data had a distinct spring neap variation. During moderate to maximum tidal velocities, finite amplitude waves dominated. These consisted of three to five oscillations of 15 min in duration separated by approximately 30 min. The Benjamin (1966) continuous stratification solitary wave model agreed well with the integrated vertical velocity field determined from the data. The core of vertical velocity migrated from near 13 m prior to 4 May to approximately 40 m later in the study, coincident with the disappearance of the strong pycnocline, detected in CTD records. During the first neap tide, smaller amplitude high frequency internal waves dominated, having numerous oscillations, with the event lasting up to 10 hours.

Table 1 indicates that the high frequency oscillations arrived from numerous directions, with most being from either cross-shore or the positive y direction (northwest). At mid-latitudes, these waves are often generated from tidal interaction with topography. Relative to our study site, potential topographic generation regions are located from 310° to 105° (Cornwallis Island) and from 170° to 240° (Griffith Island). Table 1 indicates that 17 finite amplitude events traveled across-channel, probably from topographic generation sites on Cornwallis Island while 10 other finite amplitude events propagated along-channel from predominantly the northwest where there are no known underwater topographic features that could interact with the tidal flow field. An alternative generation mechanism, in the Arctic, is tidal interaction with ice keels, a common feature. An initial examination of synthetic aperture radar pictures of the region taken in January 1992, indicated ice ridges approximately 15 km to the northwest, at the confluence of Resolute Passage and Fournier Channel. Indeed, Cummins (1994) using numerical simulations, has produced trains of solitons with similar length scales and amplitudes to those observed, which evolve from a 10 m ice keel in a flow field strength intermediate between that observed for our spring and neap tides. It is suggested that leewaves generated from tidal interaction with ice keels may contribute substantially to the formation of high frequency internal waves in the Canadian Archipelago.

Acknowledgments. The technical support of Claude Bélanger, Guy Millett and Paul Peltola in the inital data collection was greatly appreciated. Funding for the project came from the Canada-Japan Science Technology Fund through the Department of External Affairs, Canada. RFM received additional funding from the academic research program of the Department of National Defence of Canada. RGI received additional funding from NSERC and Fonds FCAR of Québec.

REFERENCES

Bayley, G. V. and J. M. Hammersley. 1946. The effective number of independent observation in an autocorrelated series. J. Roy. Statist. Soc., *B8,* 184–197.

Benjamin, T. B. 1966. Internal waves of finite amplitude and permanent form. J. Fluid Mech., *25,* 241–270.

—— 1967. Internal waves of permanent form in fluids of great depth. J. Fluid Mech., *29,* 559–592.

Benny, D. J. 1966. Long non-linear waves in fluid flows. J. Math. Phys., *45,* 52–63.

Cummins, P. F. 1994. Numerical simulations of upstream bores and solitons in a two-layered flow past an obstacle. J. Phys. Oceanogr. (in press)

Cummins, P. F. and P. H. LeBlond. 1984. Analysis of internal solitary waves observed in Davis Strait. Atmosphere-Ocean, *22,* 173–192.

Drakopoulos, P. G. and R. F. Marsden. 1993. The internal tide off the west coast of Vancouver Island. J. Phys. Oceanogr., *23,* 758–775.

Foreman, M. G. 1979. Manual for Tidal Currents and Prediction. Pacific Marine Science Report, 77-10, Institute of Ocean Sciences, Patricia Bay, Sidney, B.C.

Greenwood, K. C. 1991. Performance of an Acoustic Doppler Current Profiler in Knight Inlet, British Columbia. MSc Thesis, Physics Department, Royal Roads Military College, Victoria, British Columbia, Canada, 99 pp.

Greenwood, K. C., R. F. Marsden and J. R. Buckley. 1993. Intercomparison of an acoustic Doppler current profiler with Cyclesondes in Knight Inlet, British Columbia. Atmosphere-Ocean, *31,* 297–318.

Heathershaw, A. D., A. L. New and P. D. Edwards. 1987. Internal tides and sediment transport at the shelf break in the Celtic Sea. Cont. Shelf Res., *7,* 485–517.

Horner, R., S. F. Ackley, G. S. Dieckman, B. Gullicksen, T. Hoshiai, L. Legendre, I. A. Melnikov, W. S. Reeburgh, M. Spindler, and C. W. Sullivan. 1992. Ecology of sea ice biota. Polar Biol., *12,* 417–427.

Kubota, T., D. R. S. Ko and L. D. Dobbs. 1978. Weakly-nonlinear long internal waves in stratified fluids of finite depth. J. Hydronautics, *12,* 157–165.

Lomb, N. R. 1976. Least-squares frequency analysis of unequally spaced data. Astrophysics and Space-Science, *39,* 447–462.

Marsden, R. F., R. G. Ingram, and L. Legendre. 1994a. Currents under land-fast ice in the Canadian Arctic Archipelago. Part 2: Vertical mixing. J. Mar. Res., *52,* 1037–1049.

Marsden, R. F., B-A. Juszko and R. G. Ingram. 1994b. Internal wave directional spectra using an acoustic Doppler current profiler. J.Geophys. Res., (submitted).

Paquet, R. 1993. Internal Solitary Waves with Acoustic Applications to the Canadian Arctic and the Scotian Shelf. MSc Thesis, Physics Department, Royal Roads Military College, Victoria, British Columbia, Canada. 88 pp.

Petrie, B. 1975. M2 Surface and internal tides on the Scotian Shelf and Slope. J. Mar. Res., *33,* 303–323.

Sandstrom, H. and J. A. Elliott. 1984. Internal tide and solitons on the Scotian Shelf: A nutrient pump at work. J. Geophys. Res., *89,* 6415–6426.

Scargle, J. D. 1982. Studies in astronomical time-series II. Statistical aspects of spectral analysis of unequally spaced data. The Astrophysical J., *263,* 835–853.

Received: *21 February, 1994;* revised: *17 May, 1994.*